Development of a Robotic Lewis Rat Ankle & Foot for Advanced Testing and Evaluation of Regenerative Treatment Solutions

By: Brandon Lawrence, Maximus Cresti, Jeremiah Druckenmiller

Advisors: Dr. Shawn Russell

and Phd candidate Hudson Burke

Word Count: 5149

Number of Figures: 6

Number of Tables: 0

Number of Equations: 1

Number of Supplements: 8

Number of References: 6

Development of a Robotic Lewis Rat Ankle & Foot for Advanced Testing and Evaluation of Regenerative Treatment Solutions

Brandon C. Lawrence[a]. Maximus A. Cresti[b], Jeremiah K. Druckenmiller[c,1]

Department of Biomedical Engineering, University of Virginia, Charlottesville, VA
[1] Correspondence: vcu8ca@virginia.edu, dce6nh@virginia.edu, gag2mr@virginia.edu

Abstract

Volumetric muscle loss (VML) refers to the irreversible damage to a significant portion of muscle tissue, typically resulting from serious battlefield injuries or trauma. While several techniques have been developed to target this condition, none of them are capable of fully restoring patients to their original strength and gait patterns. The Motion Analysis and Motor Performance Laboratory at the University of Virginia led by Dr. Shawn Russell is currently studying Lewis Rats to further understand the impact of VML and design an exoskeleton capable of achieving 100% recovery for patients. This capstone project was aimed at developing an actuated physical model of a Lewis Rat ankle and foot to act as an advanced testing platform. Three servos were integrated into a simplified Stewart Platform structure, controlled via an Arduino Uno microcontroller, to recreate ankle motion with a passive foot model recreating gait force patterns via ground contact. This model was verified through motion analysis testing and alignment with existing Lewis Rat Hindlimb data. Future integration of this model into Dr. Russell's lab will allow for injury simulation and muscle force manipulation in a physical model to gain key insights into VML rehabilitation strategies.

Keywords: Volumetric Muscle Loss, Gait, Stewart Platform, Motion Analysis, Lewis Rat

Introduction

Volumetric muscle loss (VML) presents a major challenge in regenerative medicine due to the body's limited ability to repair large-scale tissue damage. The musculoskeletal system has remarkable regenerative ability, yet VML injuries exceed the body's limits, leaving patients with substantial structural and functional damage, including loss of strength, range of motion, and overall endurance. While this condition can be caused by various forms of primary and secondary trauma, a disproportionate number of VML cases affect wounded military personnel. Between 2001 and 2013, 77% of soldiers evacuated from combat sustained musculoskeletal injuries, and studies from the early 2000s indicate 65% of medically discharged personnel with orthopedic disabilities had VML[1,2]. Addressing this condition is crucial to improving the quality of life for wounded veterans.

The most prevalent treatment strategies for VML include surgical intervention, biological scaffolds, physical therapy, and bracing. Surgical intervention often refers to a functional free muscle transfer, which involves transplanting tissue from a donor site to the affected area in order to restore muscle structure and function. While such procedures have successfully restored smaller amounts of muscle mass, they fail to achieve full functional recovery. Surgical intervention is lacking in restoring the more complex movements that drive an individual's gait, which leave the patient with long-term disabilities and functional restrictions even after treatment. Donor site morbidity and limited availability of suitable donor tissue are additional risks associated with such procedures[3].

Complete muscle regeneration requires a supportive environment rich in stem cells and ECM components, which current treatments target, yet currently fail to fully achieve, resulting in poor regenerative outcomes[4]. Biological scaffolds composed of these ECM components and growth-factor delivery systems are designed to offer structural support and promote vascularization, but they are often insufficient and do not fully integrate the new tissue with the host site. In severe volumetric muscle loss (VML), where critical structures such as nerves or adjacent muscle compartments are missing, these scaffolds cannot restore

the complex muscle architecture or biomechanical properties needed for function[5]. Chronic inflammation, immune reactions, and fibrosis further block nerve ingrowth and isolate healthy muscle, preventing effective scaffold integration. Emerging approaches, such as stem cell transplantation and gene therapy, aim to overcome these limitations, but they remain in early development and have yet to demonstrate consistent functional recovery and gait restoration in VML patients.

Physical therapy holds significant promise for restoring muscle function after VML injury, especially when combined with targeted treatments like biological scaffolds or cell-based therapies. Advanced bracing can further support the affected limb and compensate for lost strength. Dr. Russell's Motion Analysis and Motor Performance Laboratory at the University of Virginia is developing neuromuscular control strategies in Lewis rats, both before and after VML injury, with the goal of translating these insights into bracing or rehabilitation technologies that restore normal gait and reduce chronic disability. Ideally, such a brace would be temporarily alleviating pain, preserving mobility, and minimizing long-term reliance on external devices[5]. To accelerate development and evaluate multiple injury scenarios, our team has built an actuated robotic model that bridges computational simulations and in vivo testing.

After a VML injury or similar musculoskeletal trauma, individuals often adopt a "local minimum" in their gait—a newly learned way of moving that is easiest on the body, to compensate for the injury constraints. Even if the muscle fibers regain full mechanical strength, the best available therapeutic interventions for recovery and physical therapy fail to restore functional gait because the body doesn't naturally relearn its pre-injury movement patterns, and there is no natural catalyst to force the body to do so. This project seeks to address this by allowing researchers to understand how to guide the body back to its original movement dynamics.

The proposed robotic rat hindlimb project closes a critical gap in VML rehabilitation by offering a high-precision, physical platform that will act as a transition point between existing computational models and future final validation animal testing. Unlike purely virtual models, this system reproduces the complex biomechanics and neuromuscular compensation patterns of a Lewis rat's gait in real time, allowing researchers to observe how different therapies affect both strength and natural movement. By translating the most promising results from thousands of simulated trials into a tangible, reproducible device, we can rapidly iterate on treatment parameters, adjusting forces, timing, and control strategies without the cost, time, or ethical concerns of large-scale animal studies. Moreover, its design lets teams vary injury severity and actuation schemes to reflect diverse VML scenarios, ensuring that therapies are evaluated under realistic, physiologically relevant conditions. This robotic model will accelerate the development and objective assessment of novel neuromuscular training protocols, streamlining the path toward clinical translation and more effective patient outcomes.

Our original project roadmap laid out four ambitious aims: (1) to develop a hybrid actuated–passive robotic replica of the lower Lewis rat hindlimb using CAD, 3D-printed and machined components, and integrated sensing; (2) to validate that model's kinematics and ground-reaction forces against in vivo motion-capture data; (3) to implement a customizable injury-simulation framework by modulating actuator strength; and (4) to ensure the device's durability and modularity through robust materials and an exchangeable architecture. Shortly after beginning our design work, we recognized that fully executing all four aims within our capstone timeline was overly ambitious. As a result, we pivoted to concentrate our efforts on completing Aim 1 (building the anatomical model) and Aim 2 (benchmarking its motion and force outputs), deferring the injury-simulation and long-term durability objectives to future teams.

Results

Assessment of Model Capabilities

Formulation of Project Goals

We began by consulting Dr. Russell and PhD candidate Hudson Burke to understand the desired ankle-and-foot mobility, research goals, and design constraints for our model. They helped us establish key performance metrics, specifying both ideal and acceptable thresholds, which guided the device's development.

Statistical Assessment of Performance

The accuracy of our design's motion (position versus time data), as compared to that of a live Lewis Rat, was measured using Pearson's Correlation Coefficient. This comparison method yields a score between -1 and +1, where +1 indicates a high similarity and -1 the opposite. The ideal result would be a less than 5% difference between our design and existing biological data, though up to a 10-15% difference is acceptable to maintain functional relevance.

We observed a Pearson's correlation coefficient of 0.9047 between our device's motion profile and the live Lewis rat data. This indicates a very strong positive relationship, meaning our model's joint trajectories closely track the biological reference. Interpreting this as a divergence of roughly 9.5% (i.e. 1-r), the performance falls just outside the "ideal" (< 5% difference) but well within our 10–15% acceptable range. Overall, these results demonstrate that the robotic model faithfully reproduces the rat's movement patterns with a level of accuracy that is functionally relevant for our VML studies.

We originally planned to compare force output between the robotic model and live rats, but in the absence of established benchmarks for normal gait forces, we deferred this analysis until those baseline studies are complete. The evaluation itself would involve a simple two-sample t-test. As with positional data, our target is a mean force difference of ≤ 5%, with up to 10–15% considered acceptable. Future capstone teams can undertake these force-comparison tests once the necessary force-output data are available.

To achieve successful communication between the sensors on the robotic hindlimb and the microcontroller to capture continuous movement, a constraint was placed on the closed-loop frequency of this design. The target for the feedback system is a frequency of 200 Hz, aligning with the standard of most motion analysis labs, with an acceptable range of +/- 15-20 Hz, which will still maintain data that conveys consistent motion. Since our design has a built-in closed loop, forgoing the complication of external sensors, our communication rate is equivalent to that of the individual servo motors. The motors we chose are the LX-824HV model, which communicates at a baud rate of 115200. Since baud rate and Hz (cycles per second) are equivalent for standard serial communication, the communication frequency is 115,200 Hz, miles above the acceptable rate.

An onboard power supply was also advised by Dr. Russell to enhance the model's mobility and accuracy. This will allow Dr. Russell and other researchers to use the model in more diverse experimental environments without the need to incorporate structures that support an off-board power setup. Preliminary designs incorporated off-board power with the goal of transitioning to a fully onboard power supply in future iterations.

First Design Iteration

Several key design features were agreed upon early in the planning process. This included ensuring full actuation of the model, discussed later in the results section, incorporating dorsiflexion and plantarflexion capabilities, and enabling modularity to facilitate quicker and easier edits or repairs. However, before any physical design or development progress could be made, thorough research into the anatomy and physiology of the rat ankle was needed. A clear understanding of dorsiflexion, plantarflexion, and the required range of motion was a critical detail that would define how the design was approached. Numerous sources were analyzed to best develop an initial, iterative design. One of the first models that we explored was the Stewart Platform, a type of parallel manipulator with 6 prismatic actuators allocated in 3 pairs around the platform's base. It offered numerous degrees of freedom in addition to precise position and motion control that closely mimicked ankle-like capabilities. However, the complexity introduced by 6 actuators proved to overcomplicate the ankle design and exceed our design objectives. Fluidum[6], a kinetic sculpture consisting of 85 robotically controlled mirrors designed by Petr Vacek, then became a key reference for our robot. Each individual panel in this device functions similarly to a Stewart Platform, but only utilizes 3 actuators. This simplified yet effective approach became a major influence on the early stages of the model's design and development.

A CAD file of the first design iteration can be seen in Figure 1. To simplify the initial development of this complex mechanical device, we assumed no size or space constraints, reserving the challenge of device miniaturization for later iterations. We focused on creating

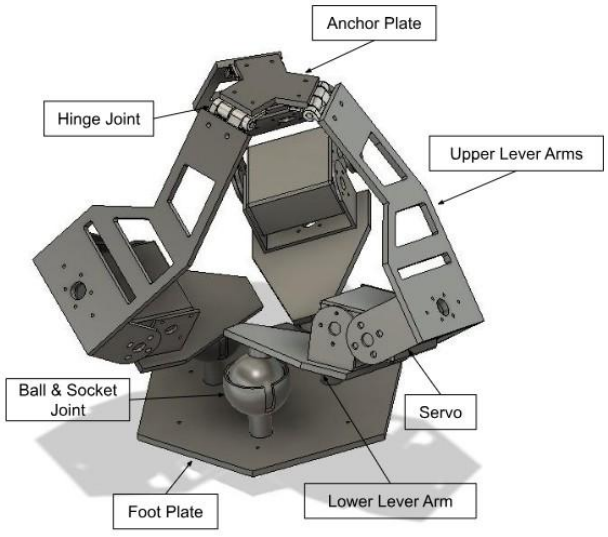

Fig. 1. Initial Design Iteration. This is a labeled CAD file of the first design iteration of the actuated ankle model.

a functional representation that maintains the overall

structure, such as length, scaled size, and connection points, while incorporating purposeful simplifications to prioritize movement over precise anatomical replication. We incorporated three Hiwonder LDX-227 digital servo motors. Each motor was coupled with a hinge and ball coupler to achieve nine degrees of freedom. The tibia and fibula structures were angled near the joint to position the ankle in plantar flexion, replicating the digitigrade posture characteristic of rats[7]. An Arduino control system interfaced with the actuators to provide precise motor control. The servo motors will offer absolute positional feedback to the Arduino for monitoring ankle joint positions. If this system had proved ineffective, we considered using linear variable differential transformers (LVDTs) as an alternative for positional feedback.

Guaranteeing Full Actuation

A fundamental requirement in robotic design is ensuring full actuation, where the number of independent actuators, in our case, servo motors, is equal to the number of degrees of freedom that need to be controlled. In this way, the system can independently manipulate each joint without relying on external forces or internal dynamics. Further, none of the joints or limbs of the robot should move unless actuated by the servos. A practical way to test full actuation is by verifying whether the robot returns to a defined resting position after carrying out a series of tasks. This became a prominent concern in the first iteration of the ankle model, as the foot plate could rotate about 45 degrees in either direction without any servo intervention. After investigating, we identified the angled design of the upper lever arm as the cause of this unwanted rotational translation.

Revised Design Iteration

The primary objective of this revised design was to achieve full actuation and reduce the size of the model. To confirm the hypothesis that the 113-degree angle in the upper lever arm contributed to the lack of actuation, the Fluidum model was revisited. We observed that the corresponding part did not exhibit an angle as our model did. Thus, the upper lever arms were redesigned to be straight and connect the servos directly to the anchor plate. Additional modifications included downsizing the anchor plate, foot plate, and lower lever arms. This not only reduced the model size, but it also centralized the connection point for all the support brackets, promoting more sensitive changes in the foot angle in response to smaller changes in servo angles. In the initial design, the lower lever arms collided when servo angles were increased. To avoid this, a new lower lever arm was introduced, providing a much smaller and more space-efficient design that permitted unobstructed movement throughout the full range of motion. A slot was also added to the socket of the rear ball joint to further enhance mobility. These iterations can be visualized in Appendix A. Finally, a simple but effective cardboard representation of the foot was developed for testing purposes. This was used until the actual foot design was completed, and it provided a valuable representation of how each servo controlled the movement of the foot. The cardboard representation of the foot can be seen in Appendix B.

Angle Mapping

With full actuation achieved, our efforts shifted toward software development to replicate the biological rat's ankle motion. Specifically, we sought to quantify the relationship between the servo angle responsible for dorsiflexion and plantar flexion and the resulting foot angle relative to the tibia. Although our model is capable of more complex movements, which may be explored in future iterations, this was the only ankle movement required by Dr. Russell's lab at this stage. Understanding how the code entered into the servos translated to the anatomical angle being replicated was critical in creating an accurate and representative robotic model. To derive this relationship, we placed the model against a gridded background, captured images across a range of servo angles, and used ImageJ to analyze the corresponding foot angles. The resulting dataset was used to generate a scatter plot and line of best fit with an R^2 value of 0.995, as seen in Appendix C. The resulting equation enabled us to convert biological dorsiflexion angles into servo commands, which were then programmed into the microcontroller for real-time motion replication.

Foot Development

The rat foot was initially created by 3D printing a mesh model provided by Dr. Russell's lab, based on the OpenSim rat model they developed. Printed at 20 times the anatomical size, this version functioned as a useful starting point, offering early insight into how the final design might come together. Using a higher-resolution anatomical scan that separated each bone[8], we simplified and reconstructed the model to include hinge joints at the second knuckle and incorporated features to allow force-generating elastic resistance, creating a passive foot design. A passive model, focusing on compliance with external forces over fine motor control of individual digits, was deemed preferable due to the unpredictable nature of the walking surface. Attempting to actuate the foot would introduce a host of complex variables that exceed the scope of this project. Further, a

rat's foot includes fourteen tarsals, which are the bones that create each digit. Designing, powering, and programming actuation in each tarsal joint would unnecessarily complicate the foot design for the current purposes of this robotic model. Thus, creating a passive foot with generic rubber bands that apply elastic force on only the metatarsal joint is a functionally adequate design that serves the purpose of this project phase.

Motion Capture Analysis

The final and most critical component of this project was utilizing the motion capture technology available in Dr. Russell's lab. This system enabled us to validate the design by comparing anatomical motion capture data collected from a live Lewis Rat to that of our robotic foot model. Multiple trials were conducted to evaluate the accuracy of the final foot design, including both static tests across a range of set angles and dynamic trials replicating full walking motion at varying speeds. The fixed-angle trials provided a general assessment of the model's accuracy. As shown in Figure 2, the output angle of the robotic foot differed from the expected value by an average of 11.74 degrees, with a standard deviation of 1.75 degrees. While this discrepancy is notable, the comparable trend in both expected and actual angle output is encouraging. To adjust for this difference, a simple calibration, such as adding 5.5 degrees to each input value, could significantly improve the alignment of expected and actual results. This offset likely stems from two primary variables: (1) human error during the initial angle mapping process that resulted in downstream inaccuracies, and (2) the weight of the block used during motion capture, which pulled the model down and increased the dorsiflexion angle during the trials.

After analyzing the general angle accuracy, we evaluated how well the model replicated real rat motion during gait cycles, a more practical and biologically relevant assessment. In Figure 3, the red-highlighted graph represents anatomical motion capture data from a walking Lewis Rat, while the light blue lines show six of the eight trials captured during testing. Two trials were omitted as statistical outliers. Examining the graph, the overall trend in our trial data closely mirrors the anatomical motion, providing strong supporting evidence for the model's validity. There is some translational error, which may be attributed to errors in the timing and speed of the trials, as the trials were taken at two different movement speeds to evaluate robotic versatility. The noise in the graphs, particularly at the peaks and troughs of the curves, is likely a result of the structural limitations of the model. Because the parts were 3D printed rather than manufactured from more rigid materials like aluminum, the system experienced wobbling and flexing at critical points in the motion, reducing overall precision.

Discussion

Future Iteration in Injury Replication

*T*he model's microcontroller and servos operate as a closed-loop feedback system, continuously reporting joint positions and enabling real-time angle adjustments. Currently, control is limited because we rely on the servos' built-in encoders. In future versions, we could decouple sensing from actuation by integrating external transducers

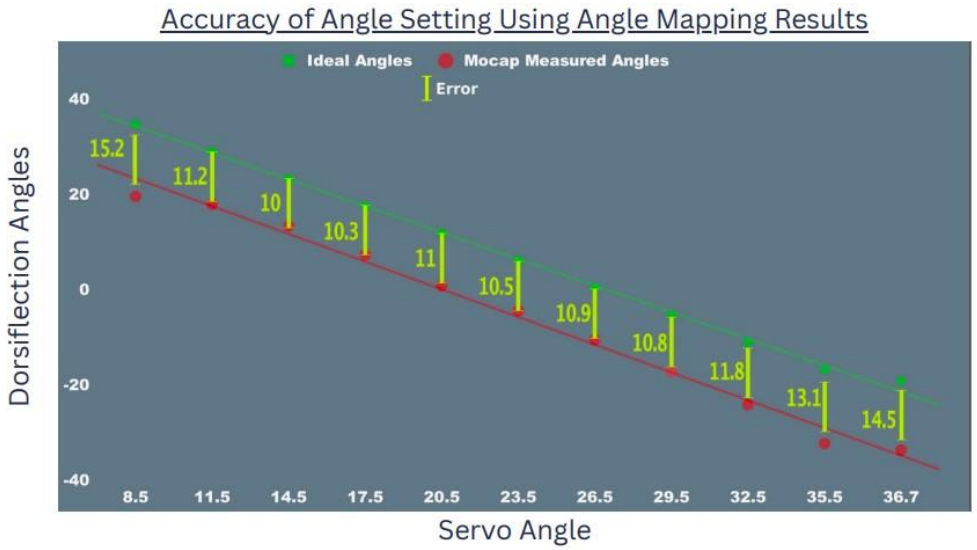

Fig. 2. Evaluation of Set Angle Values. This graph shows the difference between the intended foot model output angle and actual angle achieved for 11 trials using motion capture technology.

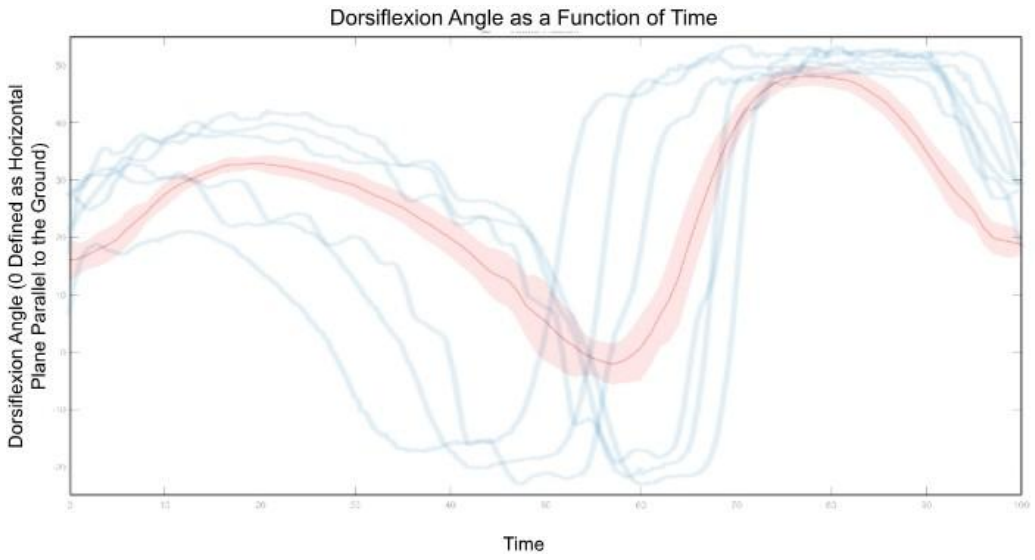

Fig. 3. Robotic Model Trials Versus Computational Data for Full Walking Motion. This graph shows the robotic ankle and foot full walking motion trials (in blue) overlayed with the full walking motion computational data of the Lewis Rat (in red).

(e.g., LVDTs) and updating the control software accordingly. By calibrating this bespoke closed loop against motion-capture data collected from VML-injured rats, the robotic model could accurately reproduce the compensatory joint behaviors observed in vivo.

Completion of the Hindlimb

We focus on the ankle and foot joints, potentially overlooking the complex interactions of the knee and hip joints, which are crucial for accurate leg positioning during gait. This omission may hinder direct comparisons between our model and a natural hindlimb, as unknown blind spots may have arisen from the oversimplification. To address these limitations, alternative design and testing could incorporate the knee and hip joints, which were designed by another capstone group, into our model to better replicate the full range of motion and inter-joint coordination observed in a rat's gait.

Maintaining Accuracy Under Influence from External Forces

We evaluated the model's motion while it was suspended, resistance-free, in the air, which does not replicate the ground reaction forces present in a rat's natural gait. These forces can meaningfully alter component trajectories, disrupt timing, or change overall movement patterns. To address this, the control software will require modifications that compensate for ground interactions. This level of analysis was beyond the current project's scope and should be undertaken in future work. Redesigning the superstructure to allow for linear or variable path movements along the ground would provide a more accurate representation for testing natural gait patterns.

Similarly, the consistent offset between our measured and ideal angles indicates that a simple code adjustment could correct the displacement. We traced this error to the block meant to replicate the foot, which was added to the ankle mechanism for motion capture. It created an external torque shown in Figure 4, only worsened by imprecise ball and hinge joints and the additional weight of the motion capture markers. This example highlights how external forces can

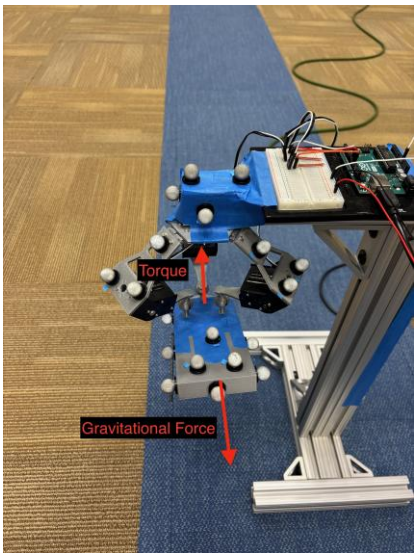

Fig. 4. External Forces Acting on Model. This visual shows the external forces that influenced an error in the motion capture testing.

distort motion and must be compensated for in future designs. Incorporating a constant angular offset in the foot's control algorithm, along with upgrading to stiffer, precision-machined metal components, will improve both accuracy and durability.

Force Generation

With our passively designed foot joint, accomplished through elastic bands spanning the hinge at the proximal interphalangeal joints, we can easily tune force output simply by adding more bands or upgrading to higher-tension elastics. These bands supply a return torque that mimics the rat's natural plantar flexion, and as we collect force-generation data, we can incrementally adjust band count or stiffness to hit our targets. Moreover, this same elastic-band approach could be extended distally to the distal interphalangeal joints or even routed along the plantar aponeurosis, allowing us to fine-tune both joint and muscle-mimetic resistance without redesigning the core mechanism.

Scale

Miniaturizing the model would enhance anatomical fidelity and accelerate gait cycles by reducing stride duration. Since the servos currently dictate the device's footprint, we can swap them for more compact actuators that deliver equivalent torque and speed. The remainder of the assembly lends itself to straightforward CAD scaling, enabling rapid iteration on a smaller form factor without redesigning the core mechanisms.

Materials and Methods

Actuated Ankle Model Construction

The servos integrated into the actuated model ankle were LDX-227 digital servos from Shenzhen Hiwonder Technology Co, Ltd. These servos have a working voltage of DC 6-8.4V with a stall current of 2.4~3A and a pulse period of 20ms. Except for the servos, screws, nuts, bolts, and washers, all remaining components of this model were printed via the Bambu Lab A1 3D printer. This printer incorporated a 0.4mm nozzle diameter and PLA filament.

Programming Integrated Servos within Ankle Model

The LDX-227 digital servos were controlled via an Arduino Uno microcontroller through the open-source Arduino Software Integrated Development Environment. Power was derived from a DC variable power supply with the voltage set to 7V, as per the working voltage requirements for the LDX-227. The configuration of the circuit board linked to the Arduino microcontroller can be seen in Appendix D. Initial testing included running all three servos through the same motion simultaneously before a more advanced code was developed to enable the ***individual control of each servo with varying degree movements and timing.***

Angle Mapping

Determining Servos 2&3 Set Points for Dorsiflexion and Plantar Flexion

An angle mapping analysis was conducted in two stages, first to determine the set point for servos 2 and 3 during normal dorsiflexion and plantar flexion control, and second to derive the relationship between the angle input into servo 1 and the output angle of the foot model. Using the OpenSim computational data on Lewis Rat walking motion, the maximum angle between the foot and horizontal ground level that the model needed to be able to achieve was 34.9 degrees, and the maximum downward angle below ground level was -19.2 degrees. The directionality of these angles is best visualized in Figure 5. With the reduced Stewart

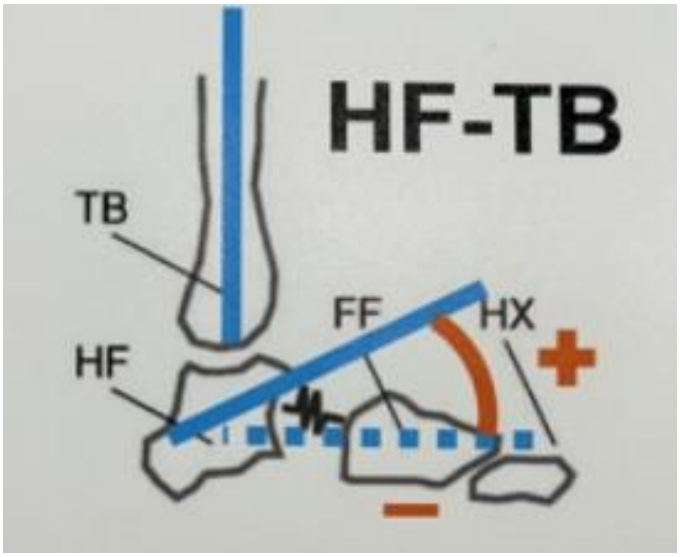

Fig. 5. Dorsiflexion & Plantar Flexion Directionality. This visual shows the positive and negative directions associated with dorsiflextion and plantar flexion.

Platform structure of this ankle model, the maximum dorsiflexion angle of the foot is achieved when servo 1 is set to 0 degrees. A number of tests were conducted to determine what angles servos 2 and 3 need to be set at to achieve the required upward angle of 34.9 degrees above the horizontal plane. These tests were carried out by programming servo 1 to be 0 degrees and servos 2 and 3 to be a test degree angle, capturing a photo of the foot output, uploading the image to ImageJ, and using the angle tool to calculate the angle between the foot and a horizontal plane. The data for this test can be seen in Appendix E. The angle of 30 degrees was chosen to be the set point for servos 2 and

3 when recreating dorsiflexion and plantar flexion motion because the maximum upward angle this allowed for was 46.9 degrees, hence including the 34.9 degree threshold with additional leniency while keeping the servos at a median position that better allows them to reach a full range of motion both positive and negative. An additional test was performed to confirm the set angle of 30 degrees was capable of achieving the plantar flexion threshold of -19.2 degrees. Setting servo 1 to 45 degrees while servos 2 and 3 were set to 30 degrees resulted in a foot output of -40.39 degrees, well over the required threshold for plantar flexion motion.

Deriving Relationship Between Servo Input and Foot Output

The relationship between angle inputs to servo 1 and the output angle of the model foot was then determined using the same ImageJ analysis method. Servos 2 and 3 were kept constant at 30 degrees, isolating the model to just dorsiflexion and plantar flexion, and servo 1 was tested through an array of angles from 5 degrees to 40 degrees. A graph of the relationship between the servo 1 set angle and the foot output angle can be seen in Appendix C. As seen in this graph, the following relationship exists.

With this relationship, the required servo 1 input could be derived for any desired angular output of the model foot.

Foot Model Construction

The development of the model foot started with a solid scan of the entire Lewis Rat foot structure provided by Dr. Russell's lab as seen in Appendix F. To create a model capable of recreating the flexion and extension of a Lewis Rat foot during normal walking motion, this scan had to be reconfigured within Fusion 360. The mesh feature was used to introduce new links as well as create space for hinge joints at key locations to allow for the appropriate movements. A hinge joint at the second knuckle of each toe allowed for the recreation of the dorsiflexion and plantar flexion bending without introducing additional degrees of freedom to other joints and bones that were not required by the scope of this project. Sockets for the ball-and-socket joints were added to the heel end of this model to allow for its connection to the ankle model. The CAD design of the foot model can be seen in Appendix G. After this model was printed using the Bambu Labs A1 3D printer, screws were drilled into either side of each knuckle joint and with washers, held in place four small rubber bands both above and below each hinge joint. This addition to the hinge joints made the resting position of the model foot completely horizontal with allowed flexion in both the positive and negative directions followed by a return to horizontal with the release of any applied force.

Motion Capture & Analysis

Performing Motion Capture Tests

In order to validate this model through motion capture analysis, the Arduino code first had to be derived to control the model through the same Lewis Rat normal walking motion from the computational studies in Dr. Russell's lab. Through the OpenSim computational data, we obtained the angle between the foot and the tibia at 5 millisecond intervals throughout the normal walking motion. These angles were then fed into the equation derived during angle mapping relating the servo 1 input to the output model foot angle to determine the code required for motion capture. Highly reflective nodes compatible with Dr. Russell's motion capture technology were then placed all around the model as well as the stand which was designed to allow the model to walk suspended in the air. A block was used in place of the model foot to create a perfectly flat surface to achieve more accurate angular results. The node placement and configuration can be seen in Appendix H. The motion capture technology used 18 cameras to achieve precise tracking and analysis of the robotic limb's movements in space over time. The first round of testing included setting servo 1 to a range of angles from 8.5 to 35.5 in 3 degree increments taking snapshots with the motion capture technology at each (servos 2 and 3 were fixed at 30 degrees during these trials). These tests were used to confirm our angle mapping process by integrating a more advanced technology to determine the angle between the foot block and theoretical tibia. The following round of testing included running the model nonstop through the array of angles taken from the OpenSim computational data (converted through the angle mapping equation). Two different speeds were tested for this full range of motion, 50 millisecond delays and 100 millisecond delays between angle shifts, and four trials were conducted for each speed.

$$[Servo\ 1\ Input\ Angle] = -0.523[Foot\ Model\ Angle] + 26.7 \quad [1]$$

Analyzing Motion Capture Data

The motion capture data was exported via an excel file including the spatial coordinates of each node at 5 millisecond intervals. This data was uploaded to MATLAB where the analysis was carried out. To interpret this data, two planes were generated, one representing the foot block and another perfectly vertical to represent the theoretical tibia. The foot block plane was defined by three nodes located on its top surface and the vertical tibia plane was defined by three nodes along the stand. These planes can be

seen in Figure 6. Normal vectors were then generated for each plane and the angles taken between the normal vectors defined the angle between the foot block and theoretical tibia. Final MATLAB graphs were derived representing the difference between each desired output angle and the actual output angle as well as the motion. path of the model foot throughout the coded walking motion versus the computational data for the same motion.

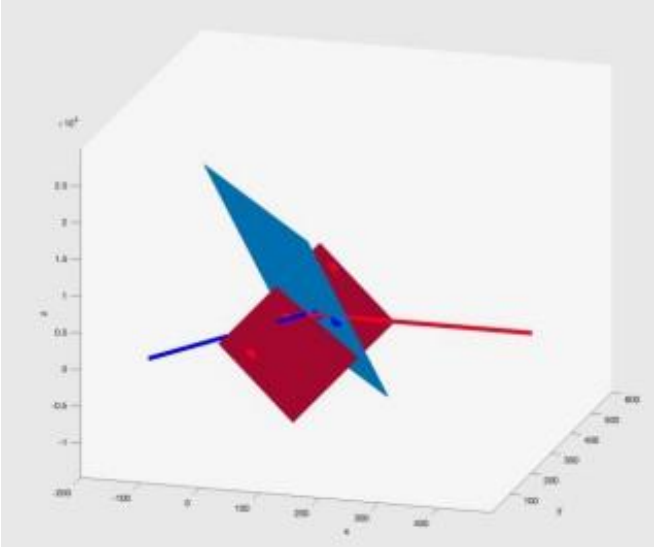

Fig. 6. MATLAB Planes for Angle Calculation. This visual shows the planes that were derived in MATLAB to be able to derive the angular data from motion capture testing.

End Matter

Author Contributions and Notes

Throughout our capstone project, all of us contributed to its development. Most of our work took place together in Dr. Russell's motion lab, where we collaborated to work through various issues we faced as the project progressed. This includes the design of the methodology and data collection, and analysis phases.

With regard to constructing the paper, Jay and Brandon wrote the abstract and introduction, setting up the results section that mostly Maximus contributed to, along with Jay. Jay also wrote the majority of the discussion section, and Brandon wrapped everything together with the materials and methods section, filling in the technical gaps in how our project and data came together. Reviewing and editing of the paper was everyone's responsibility, as we all looked through and revised the content. Finally, Brandon made a huge effort to format our paper with the figures, written sections, and appendices, ensuring that everything flowed logically.

All three of us contributed fairly equally to the development of the figures shown throughout the paper and in the appendices.

Acknowledgments

We would like to express our sincere gratitude to Dr. Shawn Russell for his invaluable guidance and feedback throughout our capstone project. We also thank the Department of Biomedical Engineering at the University of Virginia for providing the necessary resources and support. Special thanks to Hudson Burke for assisting with design specifications, data access, and insights. He provided invaluable feedback and advice throughout the development of our project.

References

1. Belmont, P. J. J., McCriskin, B. J., Hsiao, M. S., Burks, R., Nelson, K. J., & Schoenfeld, A. J. (2013). The Nature and Incidence of Musculoskeletal Combat Wounds in Iraq and Afghanistan (2005–2009). Journal of Orthopaedic Trauma, 27(5), e107.
2. Corona, B. T., Rivera, J. C., Owens, J. G., Wenke, J. C., & Rathbone, C. R. (2015). Volumetric muscle loss leads to permanent disability following extremity trauma. Journal of Rehabilitation Research and Development, 52(7), 785–792.
3. Carnes, M. E., & Pins, G. D. (2020). Skeletal Muscle Tissue Engineering: Biomaterials-Based Strategies for the Treatment of Volumetric Muscle Loss. Bioengineering, 7(3), 85.
4. Abdulghani, S., & Mitchell, G. R. (2019). Biomaterials for In Situ Tissue Regeneration: A Review. Biomolecules, 9(11), 750.
5. Grogan, B. F., Hsu, J. R., & Consortium, S. T. R. (2011). Volumetric Muscle Loss. JAAOS - Journal of the American Academy of Orthopaedic Surgeons, 19, S35.
6. "Fluidum." *Petr Vacek*, 20 Sept. 2023, petrvacek.com/portfolio/fluidum/.
7. Prodinger, P. M., Foehr, P., Bürklein, D., Bissinger, O., Pilge, H., Kreutzer, K., von Eisenhart-Rothe, R., & Tischer, T. (2018). Whole bone testing in small animals: Systematic characterization of the mechanical properties of different rodent bones available for rat fracture models. European Journal of Medical Research, 23(1), 8.

8. Baan, Guus, and Huub Maas. “Three-Dimensional Interactive Graphical Model of the Hindlimb Muscles of the Rat.” *PubMed*, National Library of Medicine, 24 Feb. 2022, karger.com/cto/article/212/3/215/836454/Three-Dimensional-Interactive-Graphical-Model-of.

Appendices

Appendix A: Iterations Made to Actuated Ankle Model

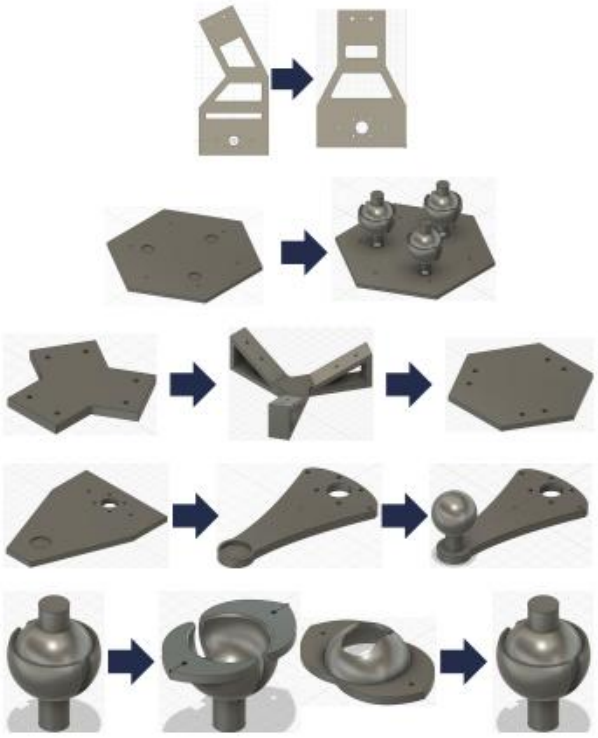

Appendix B: Cardboard Representation of Foot on Ankle Model

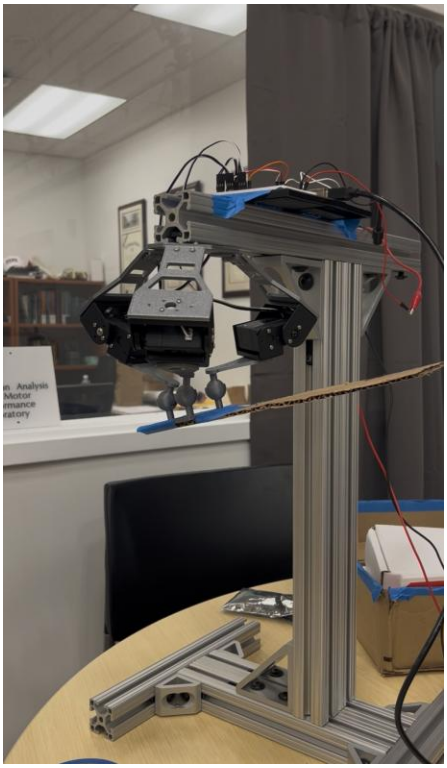

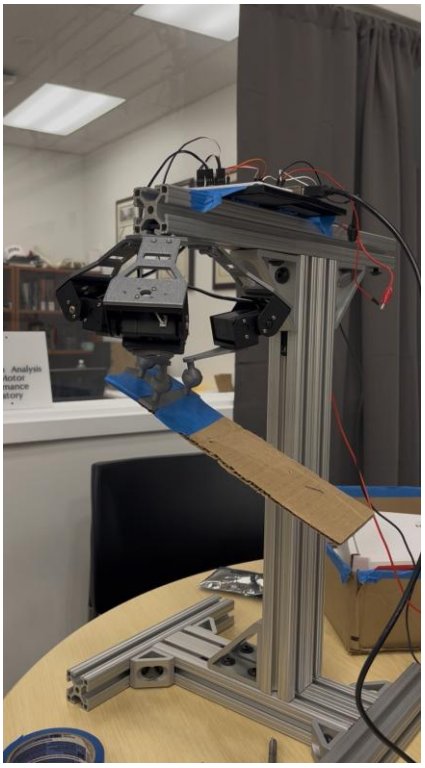

Appendix C: Angle Mapping Data

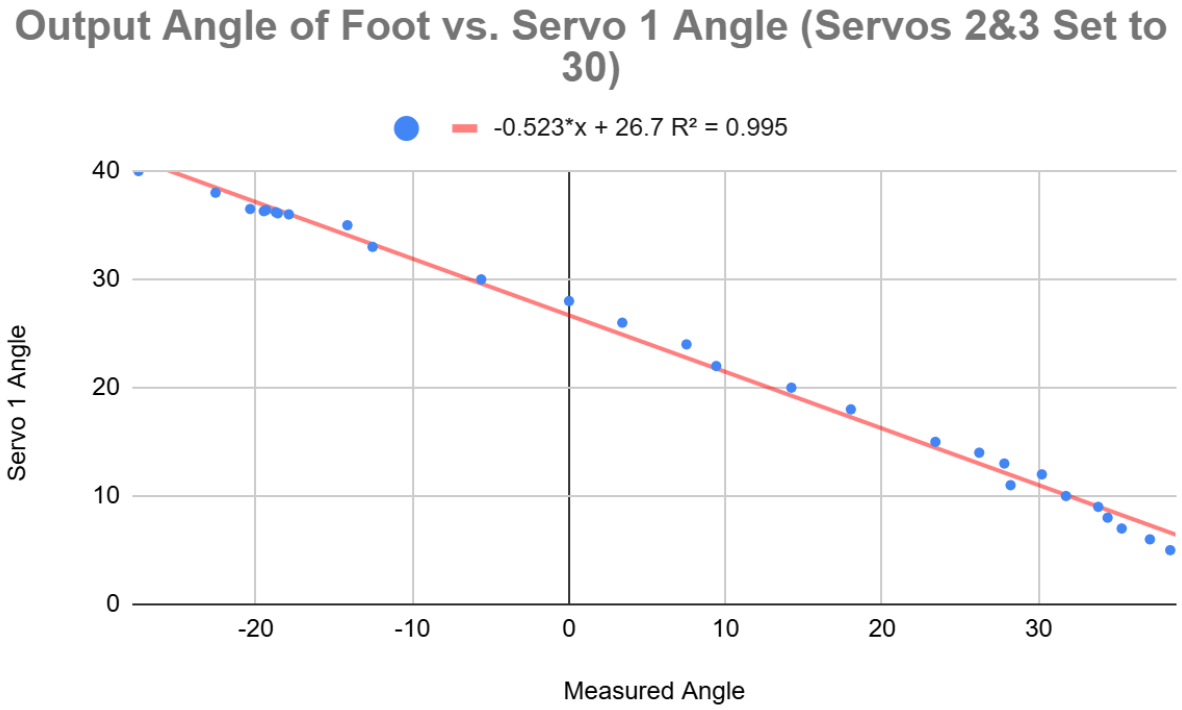

Appendix D: Arduino Microcontroller Setup

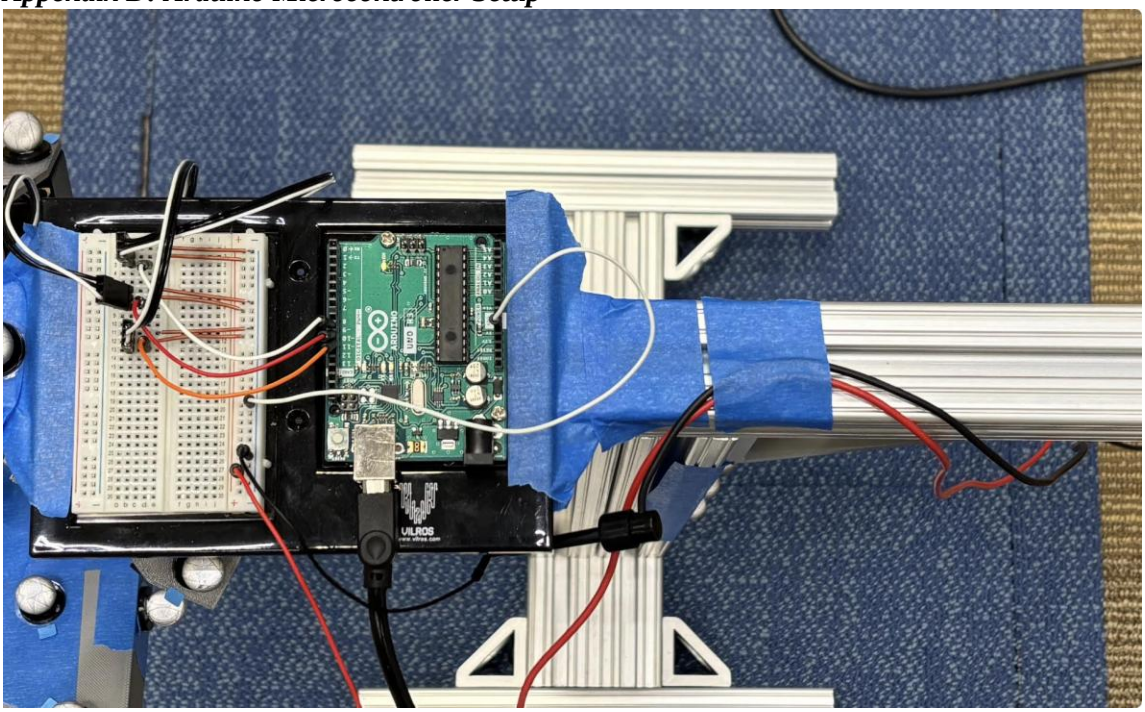

Appendix E: Data to Determine Set Angles of Servos 2&3 for Dorsiflexion and Plantar Flexion

Servo 1 Set Angle	Servo 2 Set Angle	Servo 3 Set Angle	Output Angle of Foot
0	30	30	46.9
0	32	32	48.97
0	34	34	54.39
0	36	36	59.27
0	38	38	62.95
0	40	40	65.2

Appendix F: Solid Scan of Lewis Rat Foot

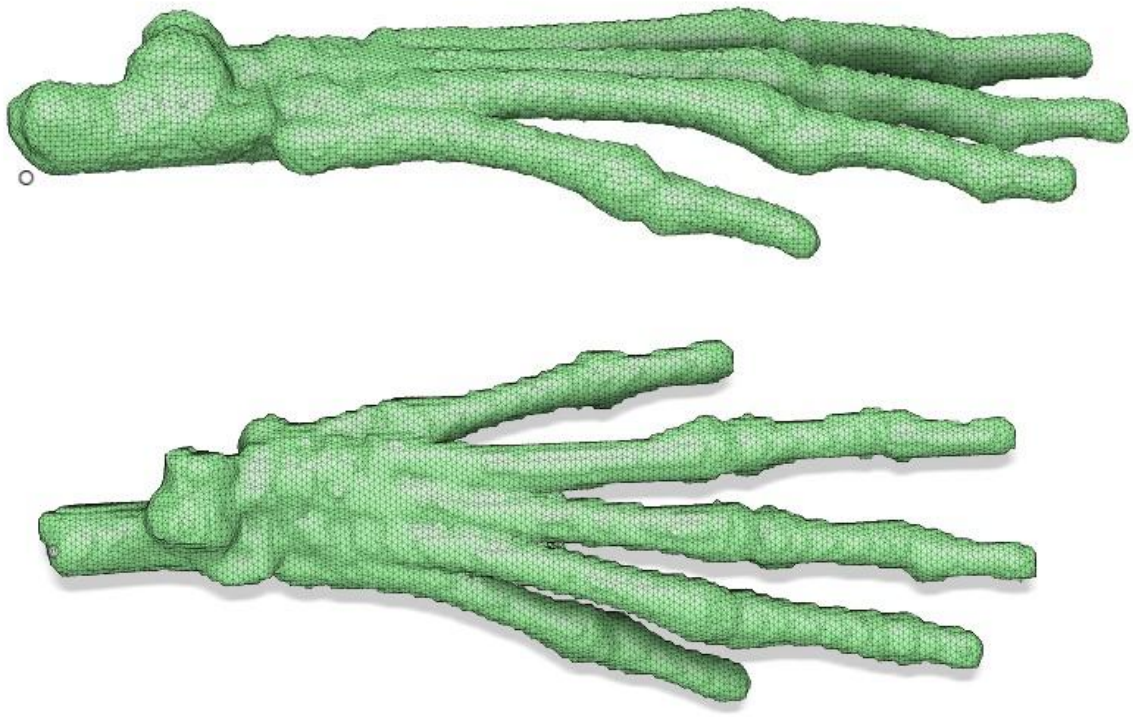

Appendix G: CAD Design of Final Robotic Foot Model

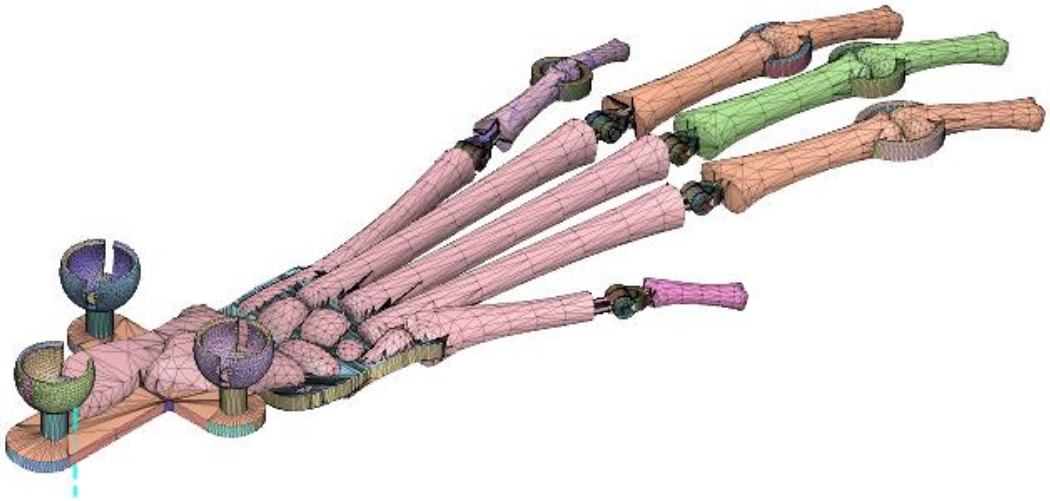

Appendix H: Motion Capture Node Placement and Configuration